Hybrid dielectric waveguide spectroscopy of individual plasmonic nanoparticles

J. Cuadra, R. Verre, M. Wersäll, C. Krückel, V. Torres-Company, T. J. Antosiewicz, and T. Shegai

Citation: AIP Advances **7**, 075207 (2017); doi: 10.1063/1.4986423
View online: http://dx.doi.org/10.1063/1.4986423
View Table of Contents: http://aip.scitation.org/toc/adv/7/7
Published by the American Institute of Physics

Hybrid dielectric waveguide spectroscopy of individual plasmonic nanoparticles

J. Cuadra,[1] R. Verre,[1] M. Wersäll,[1] C. Krückel,[2] V. Torres-Company,[2] T. J. Antosiewicz,[1,3] and T. Shegai[1,a]

[1]*Department of Physics, Chalmers University of Technology, Gothenburg 412 96, Sweden*
[2]*Department of Microtechnology and Nanoscience (MC2), Chalmers University of Technology, Gothenburg 412 96, Sweden*
[3]*Centre of New Technologies, University of Warsaw, Warsaw 02-097, Poland*

(Received 13 April 2017; accepted 4 July 2017; published online 13 July 2017)

Plasmonics is a mature scientific discipline which is now entering the realm of practical applications. Recently, significant attention has been devoted to on-chip hybrid devices where plasmonic nanoantennas are integrated in standard Si_3N_4 photonic waveguides. Light in these systems is usually coupled at the waveguide apexes by using multiple objectives and/or tapered optical fibers, rendering the analysis of spectroscopic signals a complicated task. Here, we show how by using a grating coupler and a low NA objective, quantitative spectroscopic information similar to standard dark-field spectroscopy can be obtained at the single-nanoparticle level. This technology may be useful for enabling single-nanoparticle studies in non-linear excitation regimes and/or in complex experimental environments, thus enriching the toolbox of nanophotonic methods. [http://dx.doi.org/10.1063/1.4986423]

Small metallic nanoparticles support collective oscillations of conductive electrons known as localized surface plasmon resonances. Plasmons are important for many prominent applications, including sensing[1] and catalysis[2] due to the extreme light concentration into sub-wavelength volumes. Plasmonic nanostructures are also promising for a variety of emerging optical processes and phenomena, such as non-linear effects,[3] wave-front manipulation,[4] plasmon-exciton strong coupling,[5] hot-electron generation[6] and light harvesting.[7] Additionally, metallic nanowires and nano-grooves support guided plasmonic modes and therefore can be used as subwavelength waveguides of optical signal.[8–10] To gain deeper insight into the underlying physics of these processes, single particle measurements are often needed as they overcome ensemble averaging and thereby provide deeper physical understanding.[11] Presently, the most widely spread optical, single-particle technique is dark-field scattering (DF). Albeit simple and reliable, it has a number of limitations. In particular, DF is not flexible/versatile enough to allow for advanced single nanoparticle studies, such as pump-probe and non-linear experiments, or experiments in complex environments such as optical cryostats, vacuum chambers, etc. A possible solution to these problems is the integration of plasmonic systems with low-loss dielectric waveguides. A lot of attention has been devoted in recent years to on-chip hybrid devices where plasmonic nanoantennas have been integrated with standard silicon nitride Si_3N_4 photonic waveguides.[12–20] The transparency of silicon nitride extends towards the visible, thus making it an ideal platform for observing plasmon spectroscopy in the visible and near IR, i.e. the spectral range of interest for plasmonic nanostructures. Indeed, extreme light concentration of plasmonic systems in combination with long propagation distances of dielectric waveguides promise a fruitful synergy which enables alternative illumination and light collection geometries. These hybrid systems have been already demonstrated as powerful platforms for refractometric sensing[21] and surface-enhanced Raman spectroscopy.[21,22] In these approaches light is generally coupled into the waveguide by the use

[a]Author to whom correspondence should be addressed. Electronic mail: timurs@chalmers.se

of two low NA objectives at the edges of a sample in an end-fire configuration or by near field coupling using tapered optical fiber placed close to the waveguide edges.[23] As a result, these configurations are not well suited for operation in e.g. optical cryostats and other sophisticated environments.

Here, we extend the integration of individual plasmonic nanoparticles with silicon nitride photonic waveguides using grating couplers. These couplers can be used as both the input and output channels. Such a solution has been recently used to study transmission through a waveguide[24] and we demonstrate here it is also possible to establish a direct link to the spectroscopic scattering properties of the coupled nanoparticles. This renders such hybrid systems ideal for studying individual plasmonic nanoparticles in non-linear applications and e.g. in cryostats by analyzing both transmission and scattering properties. We also discuss important aspects for optimal designs, such as momentum filtering due to low collection NA objectives and in-coupling between the plasmonic nanostructure and the waveguide.

Figure 1 shows the principal system design. The waveguide is fed from one side using unpolarized light focused by a long working distance objective on the grating. The fields of the propagating modes supported within the waveguide interact with the nanoparticle placed on top of the waveguide. Part of the light is scattered while another part propagates through towards the output end grating, where it is out-coupled into the far field and collected (as is that scattered by the particle) by *the same long working distance objective*. Hence, both the readout point and input port are addressed by the same objective, simplifying enormously the optics.

SEM and dark-field views of the system are shown in Fig. 1b. The bright field image (see e.g. Fig. S1 of the supplementary material) shows good contrast between the waveguide and the substrate but the particle is invisible in this picture. However, if the incident light beam is overlapped with the left grating, scattering by the particle (middle) and the output end (right) become clearly visible, similar to what can be detected using standard DF techniques, although the efficiency is much higher. This scheme allows also for alternative possible input-output configurations. For example, transmission can be measured at the waveguides' ends via the gratings or one could feed the waveguide via exciting the particle directly (Fig. 1b center). By coupling scattering from the particle into the waveguide, this radiation can then be collected at both output ends, thus representing a structure analogous to a beam splitter. Importantly, in all these configurations the signals/illumination are recorded/focused here using the same low NA objective ($20 \times \mathrm{NA} = 0.45$). The SEM image of the grating coupler and of the plasmonic nanoparticle embedded within the waveguide are also shown.

In order to analyze the system, we first focus on the properties of the grating coupler. It consists of several bars, whose role is to facilitate in-coupling of the far-field radiation into the waveguide, as well as, reciprocally, to out-couple light towards the microscope objective at the other end of the waveguide.

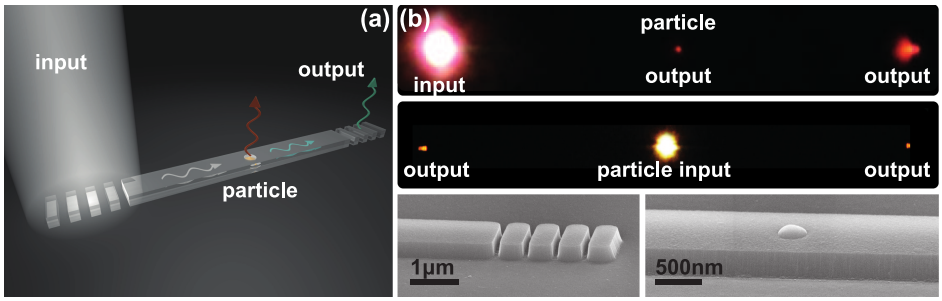

FIG. 1. (a) Sketch of the experimental setup: a Si_3N_4 waveguide equipped with grating couplers on both sides is excited by white light focused by a microscope objective. Guided modes propagate through the waveguide and are scattered by the particle as well as into the output channel. The scattered signals are collected by the same objective and sent for independent readout. (b) Realization of the proposed setup. Top: image of a fabricated hybrid plasmonic/dielectric waveguide (100 µm long) with grating in-couplers at the edges. The waveguide is illuminated from the left. The emission of the particle, and the output at the other grating are clearly visible in the center and on the right end of the waveguide, respectively. In the second image, the particle is directly illuminated instead and light emerging from both gratings is clearly observed. Bottom: tilted SEM image of the grating coupler and the nanoparticle. The analyzed waveguide grating coupler has a periodicity $\Lambda = 550$ nm and a filling factor $f = 0.75$.

In order to understand the input-output process facilitated by the grating couplers, we utilize finite-difference time domain (FDTD) calculations. Figure 2a shows the principal idea of the calculation: we launch different modes within the waveguide and study the energy g_{out} radiated by the grating coupler. This procedure on one hand allows to solve the out-coupling problem, and on the other, reciprocally we learn about the in-coupling efficiency of the supported guided modes. The width and the thickness of the waveguide are fixed to 1.2 micron and 200 nm, in accordance to experimental results. These dimensions allow the waveguide to support mainly the 0^{th} and 1^{st} order mode, concentrated in the waveguide core as shown in Figure 2b. Both polarizations are supported, although the grating coupler assures the horizontally polarized mode (TE) is coupled in more efficiently. Note that these modes are slightly asymmetric in the vertical direction due to asymmetry in the cladding material (air on top, SiO_2 on the bottom). Scattering in the upper hemi space is then collected by a monitor and the distribution of radiated power is analyzed. As an explanatory example, in Figure 2c we show the scattered pattern for the 0^{th} order mode as a function of the solid angles θ and ϕ at 710 nm. The radiation pattern is elongated and tilted ~15° with respect to the normal. The radiation pattern varies spectrally (for the full map for various wavelengths see supplementary material), meaning that if small NA objectives are used to collect the light, they also act as a momentum filter. In fact, only radiation emitted at angles θ < asin(NA) is collected, modifying the grating response. In Figure 2d, we show the out-coupling efficiency of a grating with a 550 nm periodicity (Λ) collected with two theoretical air objectives with NA = 1 and NA = 0.45. Indeed, clear differences in the spectroscopic

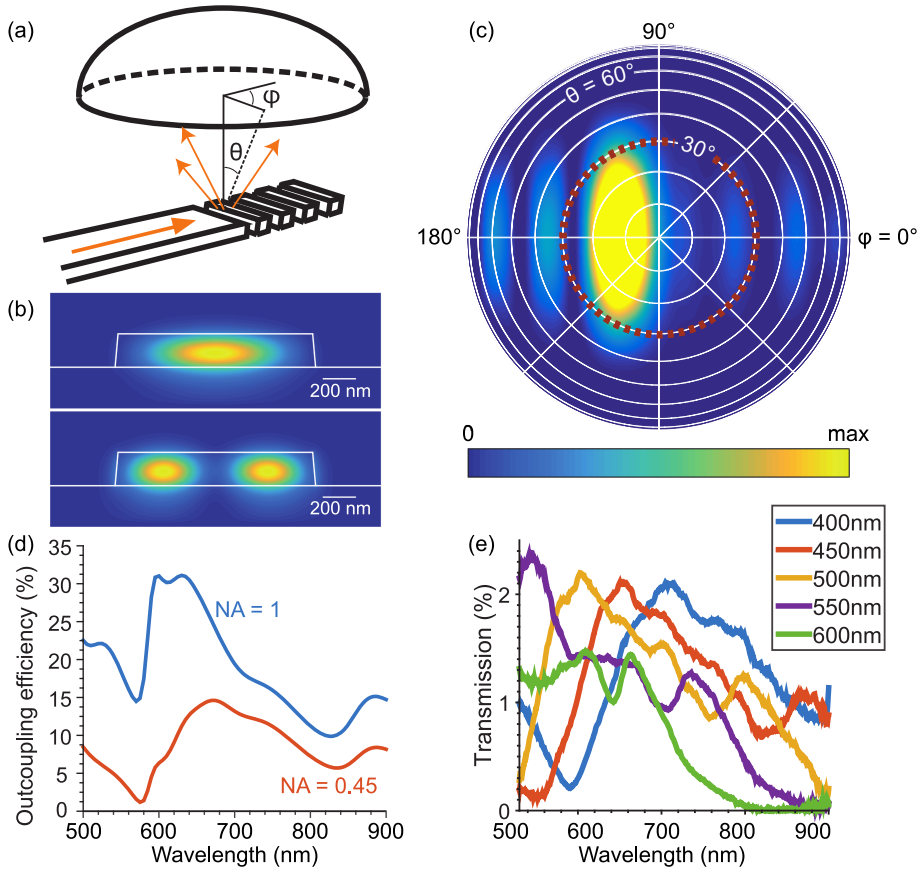

FIG. 2. (a) Sketch of the coupling simulations. Different modes are launched within the waveguide and the light scattered by the grating is monitored. (b) 0^{th} and 1^{st} order TE mode profiles calculated at λ = 710 nm. (c) Far field scattering pattern for the 0^{th} order mode. Light scattered in the region within the dashed red line corresponds to light collected by a hypothetical lens having NA = 0.45. (d) Calculated out-coupling efficiency as a function of wavelength integrated in the upper hemi space over the solid angle corresponding to NA = 1 and NA = 0.45 for $N = 4$, Λ = 550 nm and $f = 0.75$. (e) Measurement of transmission efficiency over a waveguide for different grating periodicity for $N = 4$.

out-coupling response are observed. In particular, we observe for NA = 1 that at around λ_0=630 nm the efficiency approaches 33% (number of periods N = 4, Λ = 550 nm and filling factor f = 0.75 – i.e. dielectric takes 75% while vacuum 25%), which is a relatively high number considering that the waveguide lies on a mismatched air-glass interface (and thus radiation is preferably radiated into the substrate). This value is comparable with grating coupler efficiencies in the near IR fabricated using a single-etched layer in silicon nitride.[25] The out-coupling response decreases to 14% and shifts towards λ_0 = 680 nm for smaller NA. Higher coupling efficiencies could be attained by incorporating a metal reflector underneath the silicon nitride coupler embedded in the silica buffer layer[26] or shaping the grating appropriately.[27–29] Notwithstanding, the configuration still allows a broadband performance in the spectral region that is of practical importance for plasmonics – i.e. 550 – 800 nm. This is in agreement with the 1-dB bandwidth estimate[30] $\Delta\lambda \approx \sqrt{2ln10/5}\mathrm{NA}\frac{\lambda_0}{n_w} \approx 160$nm that is based on the standard grating coupler equation. Here n_w = 1.7 is the effective refractive index of the waveguide supporting the 0^{th} order mode at 650 nm.

Experimental observations for the same configuration as a function of grating period are shown in Figure 2e. First, 200 nm Si_3N_4 films were grown by plasma enhanced chemical vapor deposition, a negative resist (MaN24-03) was exposed and the exposed pattern was transferred onto the film by a mixture of CHF_3 and Ar dry etching at low forward power to minimize the sidewall roughness. As high quality stoichiometric Si_3N_4 was grown, the losses due to absorption in the dielectric layer are minimal. As the side wall of the waveguide is invisible in the dark-field image of Figure 1b scattering losses can also be disregarded, implying that transmission (T) through the system is almost independent of the waveguide lengths within the range investigated here (60, 100 and 150 μm lengths were measured). We have fixed the waveguide length to 150 μm as being the most appropriate for working with a 20× long working distance objective (NA = 0.45). We have also studied the dependence of transmission as a function of the number of elements within the grating from N = 4 to 16 and found it to be independent of the number of grating elements. We thus fixed the number to N = 4 for an easier alignment of the fibers and the waveguide. Next, we varied the periodicity of the grating at both waveguide ends and measured transmission (see Fig. 2e). Interestingly, due to reciprocity, if the transmission through the waveguide is dominated by in- and out-coupling losses, then $T = {g_{out}}^2$ and a quantitative agreement between experiment and theory is observed once the momentum filtering effect is taken into account. The theoretical transmission through the waveguide thus should be on the order of 2%, similar to the experimental observation of ~1% where unpolarized light was used. In principle further improvement may be achieved by optimizing grating couplers.[27–29,31]

We now turn the attention to coupling between plasmonic nanoparticles and waveguides (see Fig. 3). Hybrid waveguide-plasmonic nanoparticle systems are typically characterized by analyzing the transmitted light at the output end of the waveguides. Here, we instead focus on the optical properties of single nanoparticles by measuring light scattered by the nanoparticle itself. A priori, standard DF and waveguide in-coupling may provide different information due to the different illumination conditions. In Fig. 3a-d, we demonstrate that the two methods provide very similar responses, indicating that hybrid waveguide/plasmon systems can be used for analyzing the scattering response of plasmonic nanostructures at the single-particle level analogous to DF spectroscopy.

We first compared the coupling efficiency between the 0^{th} order mode supported by the waveguide and Au nanoparticles placed either on top of a waveguide or in its core (data not shown). We found in the latter case the electric field at the center of the particles is ~4.5 times larger and consequently offers a 20-fold increase in the coupling efficiencies. We hence decided to focus on the configuration where the nanoparticle is embedded within the Si_3N_4. We then calculated the scattering cross sections of Au nanodisks inside a thin Si_3N_4 slab as a function of different disk diameters (for plane wave illumination, see Fig. 3a,b). The resonances shift toward longer wavelength for increasing nanoparticle diameter, as expected for plasmonic nanoparticles with increasing aspect ratio. The scattering cross sections were then compared to scattering from nanoparticles embedded inside a waveguide and illuminated with the fundamental TE mode (Fig. 3c,d). Light scattered into free space was measured by a monitor placed above the waveguide and corresponding to the collecting objective of NA=0.45. These spectra are very similar to the cross sections in Figure 3b, but slightly broadened due to the non-uniform field profile of the illuminating waveguide mode (see Fig. 2b). Hence, probing the particles

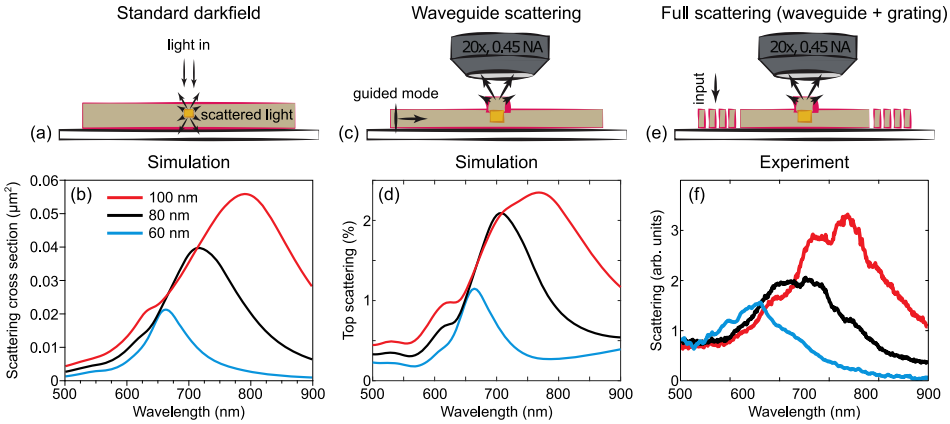

FIG. 3. Sketch of a dark scattering setup illumination configuration of an Au disk embedded in a Si_3N_4 in several different configurations. (a, b) Standard DF scattering simulated for different nanoparticle sizes. (c, d) Scattering configuration using a hybrid plasmonic waveguide system simulated for different nanoparticle sizes. (e, f) scattering spectra for individual plasmonic nanodisk of various diameters measured using the hybrid dielectric waveguide spectroscopy.

with the fundamental TE mode does indeed yield information comparable to the DF scattering cross section. It is worth mentioning here that the efficiency of the TE waveguide mode coupling to the plasmonic nanoparticle can be estimated from this scattering calculation (note nearly ~2% scattering efficiency for the largest nanodisk used in Fig. 3d). By recalling the collection efficiency of the NA=0.45 objective being about ~10%, we estimate the conversion of the TE waveguided mode into excitation of a plasmon resonance in the gold nanodisk to be around 20%. This number is further confirmed by an extinction measurement (data not shown).

We finally demonstrate the experimental feasibility of single particle scattering measurements using a hybrid waveguide/plasmonic system using grating couplers. Alignment marks and disks with different sizes were first fabricated by electron beam lithography (EBL) using positive resist (PMMA) on top of a 100 nm Si_3N_4 film followed by metal evaporation and lift off. After deposition of a second 100 nm thick Si_3N_4 film, aligned waveguides were patterned following the same method described before for the waveguides alone. Gold particles were shaped as disks with diameters of D = 60, 80 and 100 nm and height H = 60 nm to ensure that the plasmon resonance condition is fulfilled in the spectral region where the grating couplers are efficient. The scattering peak consistently shifts to longer wavelengths with increasing diameter, as expected from simulations both of Figure 3b and 3d. To obtain quantitative experimental information, however, a correct normalization procedure factor was required. Such normalization was needed to take into consideration the spectral dependency of the light source, of the detection system and of the first grating which is used to couple light into the waveguide. We normalized the signal by the scattering spectra of a hole fabricated in the center of an empty waveguide by a third EBL exposure and assuming that the scattering by the hole scales as ω^4 (See supplementary material for the details). The normalized scattered spectra are shown in Figure 2e. All features predicted by the FDTD calculations are well reproduced, however, with the minor deviations attributed to different illumination conditions in experiment and simulations (grating coupling vs. direct 0^{th} mode injection). Nevertheless, these observations clearly demonstrate that the fabricated waveguides can couple to single plasmonic nanoparticles, whose optical response can in turn be monitored spectroscopically in configurations alternative to standard DF spectroscopy but directly assessable by a single long working distance objective.

In conclusion, we have demonstrated a hybrid nanophotonic scheme that is suitable for studying spectroscopic scattering response of individual plasmonic nanoparticles in a configuration that is alternative to standard dark-field illumination. We have used FDTD calculations to estimate in- and out-coupling efficiency and grating couplers. Calculations and experimental findings agree qualitatively. This technique is a viable alternative to dark-field scattering and possesses several key advantages. In particular, this system can be used to measure individual nanoparticle spectra in complex or aggressive environments e.g. inside an optical cryostat or a chemical reaction chamber. It also

opens possibilities for pump-probe and nonlinear optical experiments, thereby enriching the toolbox of nanophotonic methods.

SUPPLEMENTARY MATERIAL

See supplementary material for additional experimental material, fabrication details and FDTD simulations for this work is available.

ACKNOWLEDGMENTS

We acknowledge financial support from Swedish Research Council (VR grants: 2012-04014 and 048701), Knut and Alice Wallenberg Foundation and the Polish National Science Center via the project 2012/07/D/ST3/02152 (TJA).

[1] B. Špačková, P. Wrobel, M. Bocková, and J. Homola, "Optical biosensors based on plasmonic nanostructures: A review," Proceedings of the IEEE **104**, 2380–2408 (2016).
[2] S. Linic, U. Aslam, C. Boerigter, and M. Morabito, "Photochemical transformations on plasmonic metal nanoparticles," Nat Mater **14**, 567–576 (2015).
[3] M. Kauranen and A. V. Zayats, "Nonlinear plasmonics," Nat Photon **6**, 737–748 (2012).
[4] E. Maguid *et al.*, "Photonic spin-controlled multifunctional shared-aperture antenna array," Science (2016).
[5] G. Zengin *et al.*, "Realizing strong light-matter interactions between single-nanoparticle plasmons and molecular excitons at ambient conditions," Phys. Rev. Lett. **114**, 157401 (2015).
[6] Y. Fang, R. Verre, L. Shao, P. Nordlander, and M. Käll, "Hot electron generation and cathodoluminescence nanoscopy of chiral split ring resonators," Nano Lett. **16**, 5183–5190 (2016).
[7] H. A. Atwater and A. Polman, "Plasmonics for improved photovoltaic devices," Nat Mater **9**, 205–213 (2010).
[8] T. Shegai *et al.*, "Unidirectional broadband light emission from supported plasmonic nanowires," Nano Letters **11**, 706–711 (2011).
[9] V. D. Miljkovic, T. Shegai, P. Johansson, and M. Käll, "Simulating light scattering from supported plasmonic nanowires," Opt. Express **20**, 10816–10826 (2012).
[10] S. I. Bozhevolnyi, V. S. Volkov, E. Devaux, J.-Y. Laluet, and T. W. Ebbesen, "Channel plasmon subwavelength waveguide components including interferometers and ring resonators," Nature **440**, 508–511 (2006).
[11] S. Syrenova *et al.*, "Hydride formation thermodynamics and hysteresis in individual Pd nanocrystals with different size and shape," Nat Mater **14**, 1236–1244 (2015).
[12] A. Espinosa-Soria, A. Griol, and A. Martínez, "Embedding a plasmonic nanoantenna into a silicon waveguide gap: Simulations and experimental demonstration," in 2016 10th International Congress on Advanced Electromagnetic Materials in Microwaves and Optics (METAMATERIALS). 106–108.
[13] M. P. Nielsen and A. Y. Elezzabi, "Nanoplasmonic distributed Bragg reflector resonators for monolithic integration on a complementary metal-oxide-semiconductor platform," Appl. Phys. Lett. **103**, 051107 (2013).
[14] O. Rubén, C. Mario, and M. Alejandro, "Fano resonances and electromagnetically induced transparency in silicon waveguides loaded with plasmonic nanoresonators," Journal of Optics **19**, 025003 (2017).
[15] L. Arnaud *et al.*, "Waveguide-coupled nanowire as an optical antenna," J. Opt. Soc. Am. A **30**, 2347–2355 (2013).
[16] C. Chen *et al.*, "Three-dimensional integration of black phosphorus photodetector with silicon photonics and nanoplasmonics," Nano Lett. **17**, 985–991 (2017).
[17] M. Février *et al.*, "Giant coupling effect between metal nanoparticle chain and optical waveguide," Nano Lett. **12**, 1032–1037 (2012).
[18] A. Espinosa-Soria, A. Griol, and A. Martínez, "Experimental measurement of plasmonic nanostructures embedded in silicon waveguide gaps," Opt. Express **24**, 9592–9601 (2016).
[19] M. Février *et al.*, "Integration of short gold nanoparticles chain on SOI waveguide toward compact integrated bio-sensors," Opt. Express **20**, 17402–17409 (2012).
[20] F. Peyskens *et al.*, "Bright and dark plasmon resonances of nanoplasmonic antennas evanescently coupled with a silicon nitride waveguide," Opt. Express **23**, 3088–3101 (2015).
[21] A. Dhakal *et al.*, "Nanophotonic waveguide enhanced Raman spectroscopy of biological submonolayers," ACS Photonics **3**, 2141–2149 (2016).
[22] F. Peyskens, A. Dhakal, P. Van Dorpe, N. Le Thomas, and R. Baets, "Surface enhanced Raman spectroscopy using a single mode nanophotonic-plasmonic platform," ACS Photonics **3**, 102–108 (2016).
[23] R. Takei, M. Suzuku, E. Omoda, S. Manako, T. Kamei, M. Mori, and Y. Sakakibara, "Silicon knife-edge taper waveguide for ultralow-loss spot-size converter fabricated by photolithography," Appl. Phys. Lett. **102**, 101108 (2013).
[24] F. Bernal Arango, A. Kwadrin, and A. F. Koenderink, "Plasmonic antennas hybridized with dielectric waveguides," ACS Nano **6**, 10156–10167 (2012).
[25] A. Z. Subramanian *et al.*, "Low-loss singlemode PECVD silicon nitride photonic wire waveguides for 532-900 nm wavelength window fabricated within a CMOS pilot line," IEEE Photonics Journal **5**, 2202809 (2013).
[26] S. Romero-García, F. Merget, F. Zhong, H. Finkelstein, and J. Witzens, "Visible wavelength silicon nitride focusing grating coupler with AlCu/TiN reflector," Opt. Lett. **38**, 2521–2523 (2013).
[27] D. Taillaert, F. Van Laere, M. Ayre, W. Bogaerts, D. Van Thourhout, P. Bienstman, and R. Baets, "Grating couplers for coupling between optical fibers and nanophotonics waveguides," Jpn. J. Appl. Phys. **45**, 6071–6077 (2006).

[28] W. S. Zaoui, A. Kunze, W. Vogel, M. Berroth, J. Butschke, F. Letzkus, and J. Burghartz, "Bridging the gap between optical fibers and silicon photonic integrated circuits," Opt. Express **22**, 1277–1286 (2014).
[29] Y. Chen, R. Halir, I. Molina-Fernandez, P. Cheben, and J.-J. He, "Hight-efficiency apodized-imaging chip-fiber grating coupler for silicon nitride waveguides," Opt. Lett. **41**, 5059–5062 (2016).
[30] C. R. Doerr, L. Chen, Y. K. Chen, and L. L. Buhl, "Wide bandwidth silicon nitride grating coupler," IEEE Photonics Technology Letters **22**, 1461–1463 (2010).
[31] G. Kewes *et al.*, "A realistic fabrication and design concept for quantum gates based on single emitters integrated in plasmonic-dielectric waveguide structures," Scientific Reports **6**, 28877 (2016).